

Journal of Biomedical Optics

SPIEDigitalLibrary.org/jbo

Single-cell photoacoustic thermometry

Liang Gao
Lidai Wang
Chiye Li
Yan Liu
Haixin Ke
Chi Zhang
Lihong V. Wang



Single-cell photoacoustic thermometry

Liang Gao,* Lidai Wang,* Chiye Li, Yan Liu, Haixin Ke, Chi Zhang, and Lihong V. Wang

Washington University in St. Louis, Department of Biomedical Engineering, One Brookings Drive, St. Louis, Missouri, 63130

Abstract. A novel photoacoustic thermometric method is presented for simultaneously imaging cells and sensing their temperature. With three-seconds-per-frame imaging speed, a temperature resolution of 0.2°C was achieved in a photo-thermal cell heating experiment. Compared to other approaches, the photoacoustic thermometric method has the advantage of not requiring custom-developed temperature-sensitive biosensors. This feature should facilitate the conversion of single-cell thermometry into a routine lab tool and make it accessible to a much broader biological research community. © 2013 Society of Photo-Optical Instrumentation Engineers (SPIE) [DOI: 10.1117/1.JBO.18.2.026003]

Keywords: cell imaging; photoacoustic microscopy; single-cell thermometry.

Paper 12486L received Jul. 30, 2012; revised manuscript received Dec. 5, 2012; accepted for publication Jan. 2, 2013; published online Feb. 1, 2013.

1 Introduction

Cellular events—such as division, gene expression and enzyme reaction – are often accompanied by intracellular temperature changes.^{1–4} Accurately measuring intracellular temperature may provide new insights into cellular signaling and metabolism. However, sensing intracellular temperature is not a trivial task, especially at the single-cell level.³

Currently, there are two major approaches to intracellular temperature sensing: one uses micro- or nano-scale thermocouples^{1,5}; the other employs temperature-sensitive fluorescent dyes,^{6,7} proteins,⁸ or nanoparticles.^{9,10} Although the thermocouple-based approach features high-temperature resolution (~0.1°C),⁵ to detect intracellular temperature changes, the tip of the thermocouple has to be inserted into cells via a micromanipulation system. This invasive operation may interrupt normal cell metabolic cycles and cause cell damage.¹¹ In addition, since only one cell can be measured at a time, the instrument is inefficient in measuring the temperature of many cells. On the other hand, the fluorescence-based approach realizes simultaneous imaging and temperature sensing with ~0.5°C resolution.¹⁰ However, most temperature-sensitive fluorescent biosensors present problems, such as sensitivity to solution pH values² and potential toxicity to cells.¹⁰

To overcome these limitations, we present a novel single-cell photoacoustic thermometric method for intracellular temperature sensing. The system is based on high-resolution photoacoustic microscopy (PAM), which measures ultrasound signals induced by light absorption.^{12–14} PAM has achieved diffraction-limited optical resolution, and was successfully applied in cellular imaging applications, e.g., detecting nanoparticle-targeted cancer cells¹⁵ and label-free imaging of cell nuclei.¹⁶ In PAM, the acquired photoacoustic (PA) image amplitude is proportional to the initial pressure rise p_0 at the absorber, induced by short-pulse laser excitation. The initial pressure rise is given by^{17–19}

$$p_0 = \left(\frac{\beta v_s^2}{C_p} \right) \mu_a F = \Gamma \mu_a F. \quad (1)$$

*These authors contributed equally to this work.

Address all correspondence to: Lihong V. Wang, Washington University in St. Louis, Department of Biomedical Engineering, One Brookings Dr., St. Louis, Missouri, 63130. Tel: 314 935 6152; Fax: 314 935 7448; E-mail: lhwang@wustl.edu

Here, β is the thermal expansion coefficient, v_s is the speed of sound in the medium, C_p is the specific heat capacity at constant pressure, μ_a is the optical absorption coefficient, and F is the optical fluence. The Gruneisen parameter Γ is temperature-dependent in water, as given by the empirical equation²⁰

$$\Gamma = A + BT, \quad (2)$$

where A and B are constants and T is the local temperature surrounding the absorber in degrees Celsius. Substituting Γ from Eq. (2) into Eq. (1) gives

$$p_0 = (A + BT)\mu_a F. \quad (3)$$

Consequently, by measuring the photoacoustic signal generated by the absorber, the local temperature can be detected. Although photoacoustic thermometry has been employed in evaluating biological tissue temperatures,^{20–22} to our knowledge this is the first time it has been used for single cell temperature imaging.

2 Results and Discussion

To demonstrate single-cell photoacoustic thermometry, an intracellular temperature-sensing experiment was carried out on HeLa cancer cells during photo-thermal heating. The HeLa cells were loaded with iron oxide micro-particles (mean diameter: 2.5 μm , PN: PI21353, Fisher Scientific) as both a photoacoustic imaging contrast agent and a photo-thermal heating source. The cells were immersed in polarization beam splitter (PBS) and imaged by a voice-coil PAM system¹³ using a 532-nm pulsed laser (pulse duration, 1 ns; pulse energy, 10 nJ; pulse repetition rate, 5 kHz). Laser pulse energy was recorded by a photodiode, and variations in the output were corrected pulse-by-pulse.

2.1 Calibration

To study the relationship between intracellular temperature and PA image amplitude, a coverslip with adherent HeLa cells was uniformly heated by a custom-made heating pad, as shown in Fig. 1(a). The heating pad was made by connecting a thin

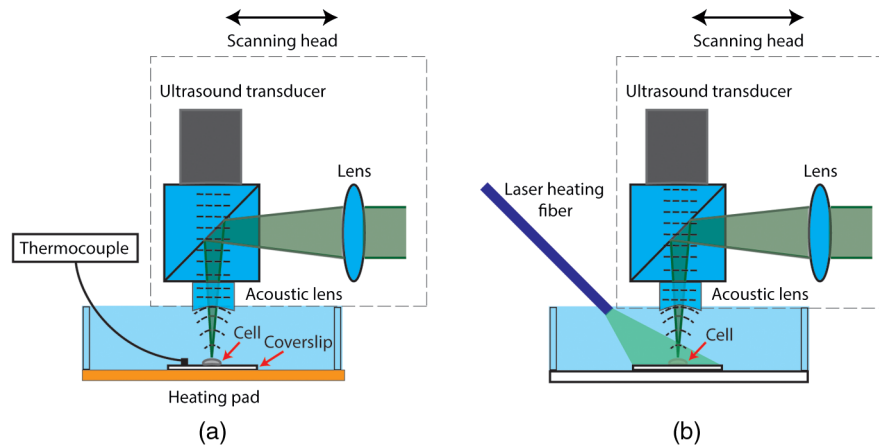


Fig. 1 System layout of PA-based cellular temperature-sensing during (a) calibration and (b) photo-thermal heating. In (b), the cell was heated by a 100-mW CW laser via a multimode fiber. The intracellular temperature was monitored by a voice-coil PAM system in real time.

metallic platform to a resistive heater (PN: HT10K, Thorlabs). A thermocouple was placed in contact with the coverslip and close to (~ 1 mm) the cells. The environment temperature was gradually raised by increasing the voltage applied to the heating pad. At each temperature, after enough time had elapsed to ensure that thermal equilibrium had been reached among the cells, the thermocouple, and the environment, a PA image was acquired and the temperature was measured by the thermocouple. Since the thermal and stress relaxation times for a $2.5\text{-}\mu\text{m}$ particle are 270 ns and 1.7 ns, respectively, which are longer than the laser pulse duration (~ 1 ns), both thermal and stress confinement conditions were satisfied. After fluence correction, the acquired PA image amplitude (peak-to-peak value of each A-line signal) was given by

$$S = k \frac{P_0}{F} = k\mu_a BT + k\mu_a A, \quad (4)$$

where k is the system's pressure sensitivity.

The measured PA signal versus temperature for a single cell is shown in Fig. 2. The PA signal of the cell was calculated by averaging all pixels within the cellular boundary. Since the internalized micro-particles were distributed in cytoplasm, the cellular boundary was estimated by applying a threshold to the acquired PA image. Four independent measurements [Fig. 2(b) to 2(e)] were carried out on the same cell pointed by an arrow in Fig. 2(a). The results indicate that the cellular temperature rise is accompanied by a linear increase in its PA signal. The slope $k\mu_a B$ and intercept $k\mu_a A$ thus can be solved by linear regression. The regressions from the four independent measurements are approximately the same, a result that proves the reproducibility of the experiment. Note that the heterogeneous distribution of particles causes a variation in PA amplitude within a cell [Fig. 2(a)]; however, since the cell was treated as a whole, the PA amplitude was averaged inside a cell. Since the cellular temperature has a one-to-one correspondence to its PA signal, the PA-recovered cellular temperature is calculated as

$$T = \frac{S - k\mu_a A}{k\mu_a B}. \quad (5)$$

In Eq. (5), the coefficients $k\mu_a A$ and $k\mu_a B$ are cell-specific, so it is critical that the calibration is done at the single-cell level.

Here the four measurements were performed approximately 10 min apart in time; however, we expect that the calibration of these coefficients remains valid as long as the loaded particles are still within the cell. Additionally, since $k\mu_a A$ and $k\mu_a B$ are calculated by linear regression, more measurements would result in a higher coefficient of determination, R^2 (presuming that random, instead of systematic, error remains a major noise source), yielding a more accurate PA-recovered temperature. However, this effort would adversely increase the calibration time, complicating operational procedures.

2.2 Single-Cell Temperature Sensing During Photo-Thermal Heating

Localized photo-thermal heating is widely used in cancer therapy.²³ Measurement of cellular temperature during photo-thermal heating is important to understanding the thermodynamics of cancer cells. The findings on cellular pathology and physiology during this process, in turn, can contribute to the development of new cancer diagnostics and therapeutics. To simulate the heating process, the output from a 100-mW CW laser (wavelength: 532 nm, PN: MLL-III-532, General Optoelectronic) was guided to the sample by a multimode fiber (PN: BFL37-600, Thorlabs) to heat up the HeLa cancer cells [see Fig. 1(b)].

The experiment was divided into three steps. First, we calibrated the relation between PA amplitude and temperature for a chosen single cell [Fig. 3(a)]. Then a control experiment without photo-thermal heating was performed to provide a baseline. The cellular temperature was monitored by the PAM at constant room temperature [see Fig. 3(b)]. The image acquisition speed was 3 s per frame. As shown in Fig. 3(b), with this imaging speed, the temperature resolution – defined as the standard deviation of the measured control temperature – was 0.2°C . Note that by using a slower imaging speed or a finer imaging step size, the temperature resolution can be further improved. Next, the heating CW laser was turned on and the cellular temperature was continuously measured by the PAM at the same acquisition speed. As seen in Fig. 3(c), the PA-recovered cellular temperature rose from 23°C to 25°C during the 300-s heating period. After the heating laser was turned off, the cellular temperature gradually decreased. To test the cells's viability after

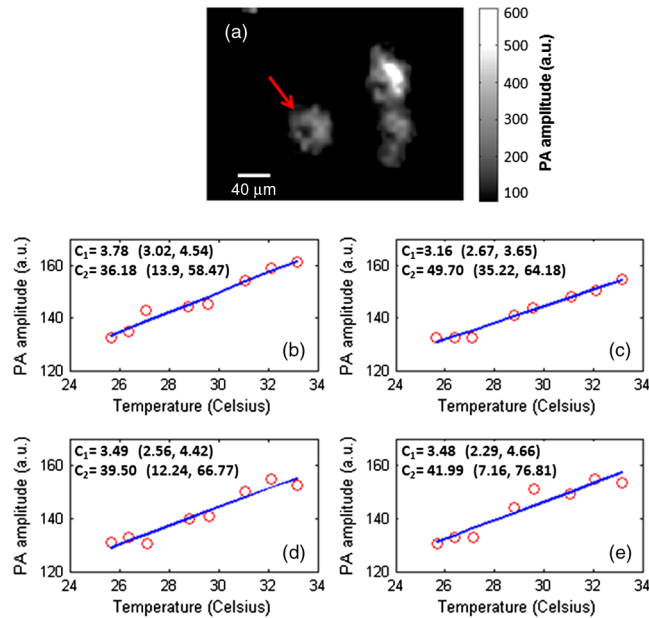


Fig. 2 PA amplitude versus temperature for a single cell. (a) Photoacoustic image of the cell at 33 °C. (b)-(e) Four independent measurements for the same cell pointed by an arrow in (a). The slope c_1 and intercept c_2 were solved by linear regression. The coefficients c_1 and c_2 were labeled with 95% confidence bounds. These measurements were made approximately 10 min apart in time.

these procedures, the cells were stained with green-fluorescence calcein-AM (cat #: L-3224, Life Technologies, Inc.) to indicate intracellular esterase activity and red-fluorescent ethidium homodimer-1 to indicate loss of plasma membrane integrity. The cells were re-imaged on a fluorescence microscope, and the results show that 84% of cells were still viable after photoacoustic imaging.

During raster scanning, repetitive probe laser pulses may cause a local temperature rise. For spheres, the thermal diffusion length d during laser-pulse interval time τ (0.2 ms) was estimated by $d = \sqrt{27\tau\alpha}$,²⁴ where α is the thermal diffusivity ($1.4 \times 10^{-3} \text{ cm}^2 \text{ s}^{-1}$). If all laser-pulse energy is absorbed and converted to heat, the temperature rise by the previous laser pulse is approximated as

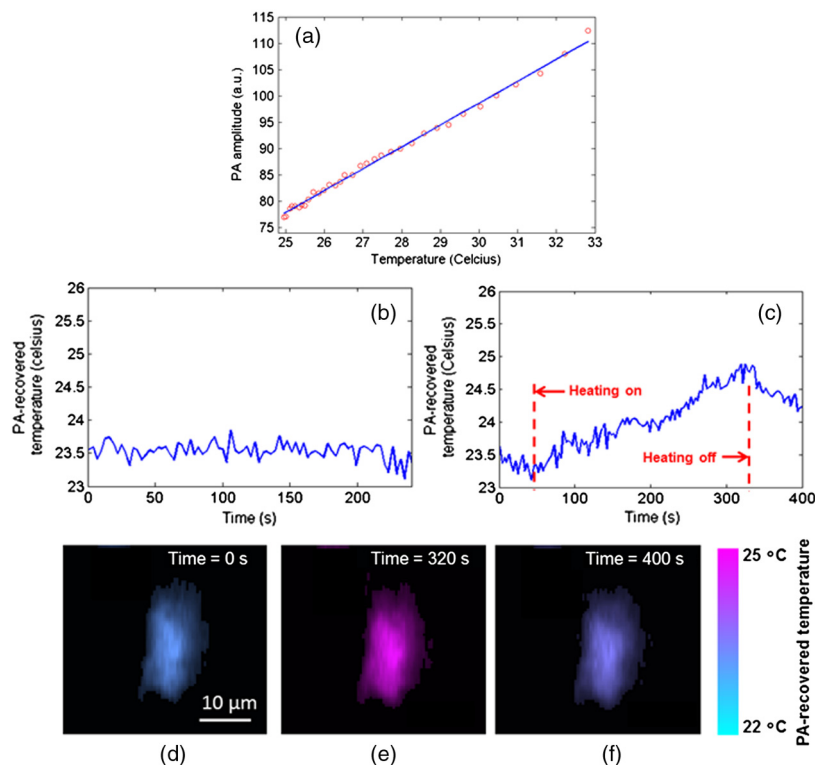


Fig. 3 Single-cell temperature-sensing during (b) control (c) photo-thermal heating. (a) shows the calibration relation between PA amplitude and temperature. The coefficient of determination, R^2 , was 0.995. (c) through (e) show the cell images during photo-thermal heating at time = 0 s, 320s, and 400s. The cell is pseudo-colored based on its PA-recovered temperatures.

$$\Delta T_1 = \frac{I}{C\rho\pi(27\tau\alpha)^{3/2}/3}, \quad (6)$$

where ΔT_1 is the temperature rise; I is the laser-pulse energy (10 nJ); C is the heat capacity ($4.2 \text{ J} \cdot \text{g}^{-1} \cdot \text{K}^{-1}$); ρ is the water density ($1 \text{ g} \cdot \text{cm}^{-3}$). The calculation gave $\Delta T_1 = 0.1^\circ\text{C}$.

With n previous laser pulses, the total temperature rise became

$$\Delta T = \Delta T_1 \sum_{i=1}^n i^{-3/2}, \quad (7)$$

where i is the index of laser pulse in the current measurement. Thus, the estimated total temperature rise due to all the laser pulses ($n \approx 1000$) that were delivered to scan across a cell was $\sim 0.3^\circ\text{C}$, which is much less than the cell temperature. If a smaller temperature rise is desired, lower laser-pulse energy and a slower pulse repetition rate may be used.

We also evaluated the dependence of the system's pressure sensitivity on the coupling water's temperature. First, since the ultrasound transducer was in the air and the room temperature was considered stable during the experiments, the transducer's pressure sensitivity can be considered constant. Next, the coupling water's temperature change may alter the speed of sound, acoustic focal distance and focal spot size, so the system's pressure sensitivity can be affected. Here we estimated the acoustic focal distance and spot size at 25°C and 33°C with an assumption of a uniform temperature distribution in the coupling water. The focal distance was calculated from

$$l = \frac{v_q}{v_q - v_w} R, \quad (8)$$

where l is the focal distance, v_q is the sound speed in acoustic lens (quartz), v_w is the sound speed in water, and R is the radius of the acoustic lens. The focal diameter d is computed from

$$d = 0.71 \frac{v_w 2l}{fD}, \quad (9)$$

where f is the acoustic frequency, and D is the outer diameter of the acoustic lens. When temperature increases from 25°C to 33°C , the focal distance and the focal diameter decreases by 0.5% and 1.7% respectively. In linear approximation, the total temperature's effect on the system sensitivity was estimated as $(1 - 0.005) \times (1 + 0.017)^2 - 1 = 2.9\%$. At the same time the measured PA amplitude increased by 41%, which was 13 times higher than the system's pressure sensitivity change. Therefore the effect of coupling water's temperature change on the system's pressure sensitivity is negligible.

The sensitivity to local temperature in PA imaging rises from the intrinsic photoacoustic generation mechanism. Consequently, the PAM-based method features the unique advantage of not requiring additional temperature-sensitive contrast agents to sense cellular temperature – the loaded iron oxide particles simultaneously play dual roles as a photo-thermal heating source and a local temperature sensor. This simplifies the experimental procedures and setup, as compared to the fluorescence-based approach.⁸

The single-cell photoacoustic thermometry requires that the cell stays in the same solution and cellular environment during calibration and temperature measurement experiments. For *in-*

vivo studies, since the tissue surrounding the cell may also contribute to the PA signal,²⁵ the correspondence between PA amplitude and cellular temperature acquired by *in-vitro* calibration experiment may not be applicable. To reduce the effect of surrounding tissue on the *in-vivo* cellular temperature measurement, one can minimize the ratio of the tissue's absorption to the sensing particle's absorption by choosing an exciting wavelength.

3 Conclusions

In summary, a novel PAM-based method is presented for single-cell temperature sensing. With 3-s-per-frame imaging speed, the PAM-based method has achieved a temperature resolution of 0.2°C in a photo-thermal heating experiment. To the best of our knowledge, this is the first time that photoacoustic temperature-sensing has been realized at the single-cell level.

Compared to other cellular temperature sensing methods, the PAM-based approach has the advantage of not requiring custom-developed temperature-sensitive biosensors. One can choose commercially available absorptive dyes or particles as the temperature-sensitive agent in cellular imaging applications. Although not demonstrated in this paper, by tuning the imaging laser wavelength, endogenous cellular absorption contrasts, such as hemoglobin, melanin, lipid, DNA/RNA, and protein,^{12,16} may also be employed for intracellular temperature-sensing without cellular staining. The feasibilities will be investigated in the future. The presented photoacoustic thermometry should make single-cell temperature sensing accessible to a much broader biological research community.

4 Methods

4.1 Cellular Sample Preparation

The HeLa cells were maintained in Dulbecco's Modified Eagle Medium with 10% fetal bovine serum, 2 mM glutamine and 1% penicillin/streptomycin supplement. The cells were incubated at 37°C , in 5% CO_2 , and were divided every 72 h. After being dispersed in 0.25% EDTA-trypsin, they were seeded at $2\text{--}4 \times 10^4$ cells/ cm^2 . As a PA-imaging contrast agent, iron oxide micro-particles (PN: PI21353, Fisher Scientific) were added to the cell medium in a concentration of 0.5 pM and incubated for 24 h. The diameters of these particles range from 1 to 4 μm with a mean of 2.5 μm . Since the amount and rate of internalization were sufficient, the particles were not coated to increase uptake. Coverslips with adherent cells were washed with PBS before imaging. The optical microscopic imaging showed that the micro-particles were distributed in cytoplasm.

4.2 Photoacoustic Microscopy

A recently developed voice-coil PAM system¹³ was employed to acquire the temperature-dependent cellular images. The voice-coil PAM system consists of a PA probe and a raster scanner. In the PA probe, short laser pulses (PN: 10-200-532, Elforlight Ltd.) were focused onto the sample surface through a set of optics. The generated photoacoustic signals were collected by an ultrasound lens (6 mm aperture, 0.5 NA in water) and received by a high-frequency ultrasound transducer (PN: V2022 BC, Olympus NDT). To achieve high sensitivity, the optical and acoustic foci were confocally and coaxially aligned. The photoacoustic probe was mounted onto a voice-coil-based scanner (PN: VCS-1010, Equipment Solutions) to

implement fast imaging. In experiments, the sample was scanned at a 10-Hz cross-sectional imaging speed and a 1/3-Hz volumetric imaging speed. The lateral resolution was measured as 3.4 μm . A higher spatial resolution is possible by increasing the optical numerical aperture.

Acknowledgments

This work was sponsored by the National Institutes of Health (NIH) under grants R01 EB000712, R01 EB008085, R01 CA134539, U54 CA136398, R01 CA157277, and R01 CA159959. L. V. Wang has a financial interest in Microphotoacoustics, Inc. and Endra, Inc.; however, neither provided support for this work.

References

1. M. Suzuki et al., "Microscopic detection of thermogenesis in a single HeLa cell," *Biophys. J.* **92**(6), L46–L48 (2007).
2. O. Zohar et al., "Thermal imaging of receptor-activated heat production in single cells," *Biophys. J.* **74**(1), 82–89 (1998).
3. B. B. Lowell and B. M. Spiegelman, "Towards a molecular understanding of adaptive thermogenesis," *Nature* **404**(6778), 652–660 (2000).
4. E. Tanaka et al., "Microcalorimetric measurements of heat-production in isolated rat brown adipocytes," *Biochem. Int.* **26**(5), 873–877 (1992).
5. C. L. Wang et al., "Determining intracellular temperature at single-cell level by a novel thermocouple method," *Cell. Res.* **21**(10), 1517–1519 (2011).
6. C. F. Chapman et al., "The use of exogenous fluorescent-probes for temperature-measurements in single living cells," *Photochem. Photobiol.* **62**(3), 416–425 (1995).
7. K. Okabe et al., "Intracellular temperature mapping with a fluorescent polymeric thermometer and fluorescence lifetime imaging microscopy," *Nat. Commun.* **3**, 705 (2012).
8. J. S. Donner et al., "Mapping intracellular temperature using green fluorescent protein," *Nano. Lett.* **12**(4), 2107–2111 (2012).
9. F. Vetroni et al., "Temperature sensing using fluorescent nanothermometers," *Acs. Nano.* **4**(6), 3254–3258 (2010).
10. C. Gota et al., "Hydrophilic fluorescent nanogel thermometer for intracellular thermometry," *J. Am. Chem. Soc.* **131**(8), 2766–2767 (2009).
11. I. Lafflaflan and M. B. Hallett, "Gentle microinjection for myeloid cells using SLAM," *Blood* **95**(10), 3270–3271 (2000).
12. L. H. V. Wang and S. Hu, "Photoacoustic tomography: *in vivo* imaging from organelles to organs," *Science* **335**(6075), 1458–1462 (2012).
13. L. D. Wang et al., "Fast voice-coil scanning optical-resolution photoacoustic microscopy," *Opt. Lett.* **36**(2), 139–141 (2011).
14. S. Hu, K. Maslov, and L. V. Wang, "Second-generation optical-resolution photoacoustic microscopy with improved sensitivity and speed," *Opt. Lett.* **36**(7), 1134–1136 (2011).
15. S. Mallidi et al., "Multiwavelength photoacoustic imaging and plasmon resonance coupling of gold nanoparticles for selective detection of cancer," *Nano. Lett.* **9**(8), 2825–2831 (2009).
16. D. K. Yao et al., "*In vivo* label-free photoacoustic microscopy of cell nuclei by excitation of DNA and RNA," *Opt. Lett.* **35**(24), 4139–4141 (2010).
17. L. V. Wang and H.-i. Wu, *Biomedical Optics: Principles and Imaging*, Wiley-Interscience, Hoboken, NJ (2007).
18. G. Paltauf and P. E. Dyer, "Photomechanical processes and effects in ablation," *Chem. Rev.* **103**(2), 487–518 (2003).
19. B. T. Cox and P. C. Beard, "Fast calculation of pulsed photoacoustic fields in fluids using *k*-space methods," *J. Acoust. Soc. Am.* **117**(6), 3616–3627 (2005).
20. I. V. Larina, K. V. Larin, and R. O. Esenaliev, "Real-time photoacoustic monitoring of temperature in tissues," *J. Phys. D: Appl. Phys.* **38**(15), 2633–2639 (2005).
21. S. M. Nikitin, T. D. Khokhlova, and I. M. Pelivanov, "Temperature dependence of the photoacoustic transformation efficiency in *ex vivo* tissues for application in monitoring thermal therapies," *J. Biomed. Opt.* **17**(6), 061214 (2012).
22. R. Brinkmann et al., "Real-time temperature determination during retinal photocoagulation on patients," *J. Biomed. Opt.* **17**(6), 061219 (2012).
23. X. H. Huang et al., "Plasmonic photothermal therapy (PPTT) using gold nanoparticles," *Laser Med. Sci.* **23**(3), 217–228 (2008).
24. R. R. Anderson and J. A. Parrish, "Selective photothermolysis: precise microsurgery by selective absorption of pulsed radiation," *Science* **220**(4596), 524–527 (1983).
25. V. N. Inkov, A. A. Karabutov, and I. M. Pelivanov, "A theoretical model of the linear thermo-optical response of an absorbing particle immersed in a liquid," *Laser Phys.* **11**(12), 1283–1291 (2001).